Characterization of a Class of Soft Bending Arms

Gina Olson[1], Brian Woronowicz[2] and Yiğit Mengüç[3]

***Abstract*— Bending permits soft arms to access a workspace that is not colinear with the initial arm axis; the size and shape of this space depends on the characteristics of the soft arm. Soft bending actuators and arms have developed for specific applications, but not characterized for the general relationship between design variables and performance. This paper defines a class of soft bending arms based on its design, considering the arm as a system constructed from many contracting actuators organized into segments. A modular segment design is presented, and seven variants of this design were constructed and tested for bend radius, bend direction, lateral stiffness and contraction. The variants isolate system parameters, in this case, arm radius and number of actuators within a given segment, to quantify how these parameters affect performance. A trade-off was found between lateral stiffness and bend radius, which can be controlled by altering the arm radius or the number of actuators. Bend direction was found to be coupled to both bend radius and arm load. Finally, a three-segment arm following a bio-inspired design is presented to demonstrate how the experimental results apply to soft robot system design.**

I. INTRODUCTION

The revolute or spherical joints used in traditional robot arms permit access to a workspace beyond that which is colinear with the initial orientation of the arm. In soft robot arms, continuum bending performs the same function. An arm that can contract, extend and twist about or along its own axis is still bound to a narrow workspace extending forward and back from its tip. Bending, though, changes the tip axis, the shape, and, in some cases, the stiffness of the arm. This change in shape of the soft robot arm often amounts to a change in the structure and loading, as actuators that were soft and compliant are inflated, compressed or tensioned. Traditional methods of load and motion analysis, based on rigid links actuated precisely to known relative angles, do not apply. The limits of a given soft arm's workspace, and its ability to manipulate objects and apply loads within that space, still depend on the characteristics of the arm, but are not straightforward to determine.

Soft robots trade power and precision for safety and delicacy. Soft robots are typically made of elastomers such as silicone or polyurethane, and reinforced by fibers or fabric. The combination of the design and the materials used distribute actuation and load. Pneumatic, hydraulic and electric actuators are commonly used, but, when coupled with soft materials, these actuators naturally produce much lower loads than their traditional robotics counterparts. Despite this, or indeed because of it, soft robots are often proposed for grippers, swimming robots and crawling robots, due to their ability to conform to their environment and distribute deformation [1], [2], [3].

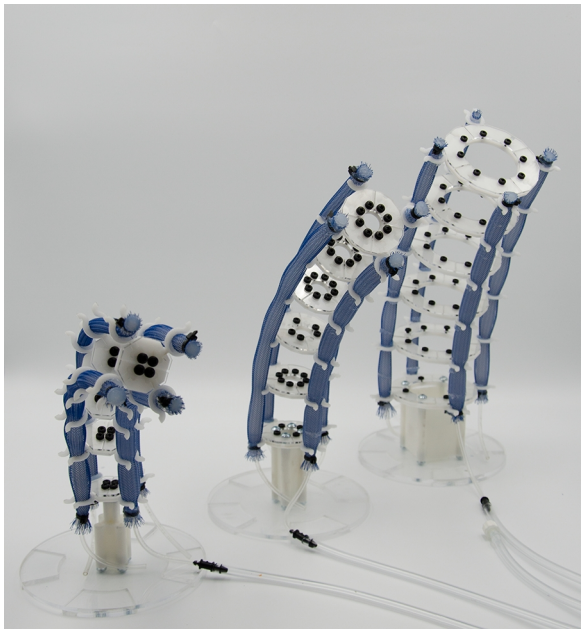

Fig. 1. Three segments developed for testing, pressurized to their (approximately) minimum bend radius. The design of each of the McKibben actuators is the same, but the diameter of the arm varies. From left to right, the arm diameters are: 45 mm, 60 mm and 90 mm.

The set of soft bending actuators and arms that have been developed span an impressive range in size and style, from a two meter long tendon-actuated vine-inspired robot, to a combination fluid-actuated, jamming-stiffened segmented arm, to a gripper where each finger is composed of four linear soft actuators activated in groups to generate bending [4], [5], [6]. Even with this variety, most of these systems can be organized into two groups based on their working principle. Regardless of actuation by air, water or electricity, single-actuator bending can be created by generating a strain imbalance between two sides of the actuator. Examples include: (1) embedding a strain limiting layer such as fabric or a much stiffer elastomer (which eliminates the possibility of adding extension or contraction) [7], (2) altering the geometric profile to lower the stiffness on one side [8], or (3) molding multiple chambers but only inflating one [9],[10]. Single actuator bending, though simple and popular,

[1]G. Olson is a Graduate Student in mLab at Oregon State University's Collaborative Robotics and Intelligent Systems Institute (e-mail: olsongi@oregonstate.edu).

[2]B. Woronowicz is an Undergraduate Researcher Student from University of Maryland, Baltimore County (e-mail: bworono1@umbc.edu).

[3]Y. Mengüç is mLab's Lab Director and an Assistant Professor at Oregon State University's Collaborative Robotics and Intelligent Systems Institute (e-mail: yigit.menguc@oregonstate.edu). Y. Mengüç is also a Research Scientist at Facebook Reality Labs.

scales up poorly. Dieletric elastomeric actuators, which must be stacked or rolled, would be heavy, and pneumatic and hydraulic actuators, with such a large cavity, would be flimsy and slow to inflate.

The second group also creates a strain imbalance, but the imbalance is generated by individual contracting or extending actuators combined into a system. Examples include a variable stiffness gripper and the associated bending arm segment presented [6], [11], a multi-segment “third-arm" [12], OctArm [13] and STIFF-FLOP [5]. This type of arm is, to an extent, representative of boneless limbs, such as octopus arms, and is more easily integrated with other sets of actuators to generate additional motions [14]. Twist has been implemented into a soft arm with hard and soft components, and extension and contraction have been added using pneumatic and shape memory alloy actuators [15], [16], [17], [18], [19]. The actuator cavity size of actuator-system arms is not necessarily related to arm size, and the space between actuators can be used for supporting structure, other actuators, or left empty to minimize stiffness.

This paper focuses on bending generated by systems of actuators. Many-actuator bending arms are hierarchical structures, and, within a range, global behavior can be tuned independently of the actuator. While most of the soft arms noted above were characterized to identify the behavior and potential of its particular design, studies have not extended to characterizing system-level variants of the same design. This paper considers variants of one arm segment design, and characterizes the contraction, minimum bend radius and lateral stiffness of those variants, to identify how whole-arm design parameters affect performance. The segment’s minimum bend radius is strongly correlated to the whole arm’s workspace size, while lateral stiffness is correlated to performance under load. The contributions of this work are:

1) Development of a modular arm design that allows quick reconfiguration.
2) Measurement of the effect of arm diameter and the number of actuators on stiffness and contraction.
3) Experimental measurement of the relationship between pressure, bend radius and direction, and investigation of the coupling between bend radius and direction.

This paper begins by presenting a refined manufacturing procedure for McKibben actuators (Section II), which are the actuators selected for the arm. The arm, which is described in Section III, is formed by connecting actuators to radial support plates with keys, to allow modularity in arm radius and the number of actuators within each segment. Approximately thirty actuators were made, and, from this lot of actuators, seven variants were made and tested for contraction, single-actuator bending, dual actuator bending and stiffness under gravity loading (Section IV, V). Three of the variants are shown in Figure 1. Finally, a three-segment arm was constructed to demonstrate the potential applications of these results (Section VI).

II. ACTUATOR FABRICATION

The first step in arm development was to select an actuator type. No specific actuator was required, merely the ability to contract or extend. McKibben actuators were selected for their simplicity, low cost and popularity in soft robotics. These actuators have a comparatively low contraction ratio, but high initial force. McKibben actuators are nicknamed “air muscle" for the similarity of their force profile to that of biological muscle. McKibben actuators belong to a broader class of pneumatic actuators that include extensile actuators, but in this case the traditional, contracting, version was selected to avoid buckling. This selection is not intended to argue that McKibben actuators are the ideal choice, merely a convenient one.

McKibben actuators are constructed from a soft elastomeric bladder surrounded by a reinforcing sleeving. The McKibben actuators used in this work were molded from EcoFlex 00-30 and reinforced by an off-the-shelf expandable sleeve made of polyester plastic (McMaster #9284K2). Actuator dimensions were selected early and used throughout the study. The cylindrical elastomeric bladders had an inner diameter of 6 mm and a wall thickness of 1.5 mm. Because the study required actuators with consistent properties, a refined manufacturing process was developed to eliminate air bubbles within the bladder walls. The key refinements were: a mold with a large contact area that bolted shut, use of gravity to fill the cavity, timed degassing and use of a sheathing jig. The steps to manufacture a McKibben actuator, from molding to key attachment, were:

1) The mold was cleaned with isopropyl alcohol and released with Ease Release 200. The steel mandrel minimizes warp and deflection. See Figure 2.(a).
2) The mold was bolted shut to prevent silicone leak at the parting line, and a small amount of clay was used to secure and seal the funnel to the mold.
3) Ecoflex 00-30 was mixed and defoamed in a Thinky mixer. The mold was oriented vertically, and the mixed silicone poured into the funnel. The silicone was allowed to flow down the mold, pushing the air out a vent hole at the base. When the elastomer reached the bottom, the hole was plugged with clay.
4) The mold was placed in a vacuum chamber and degassed. Through trial and error, it was found that degassing at -750 mmHg for five minutes was optimal for removing air bubbles. If degassed too little, not all air bubbles were removed. Conversely, if degassed too long, it was observed that the EcoFlex 00-30 would cure faster. The authors suspect this is caused by components of the uncured silicone boiling off.
5) The mold was oriented vertically and the silicone allowed to settle. Commonly, a few large air bubbles remained, coalesced from smaller bubbles, but these most often floated out. See Figure 2.(b).
6) The mold was left to cure at room temperature for a minimum of four hours, and then the bladder was removed from the tool (Figure 2.(c)). Once detooled,

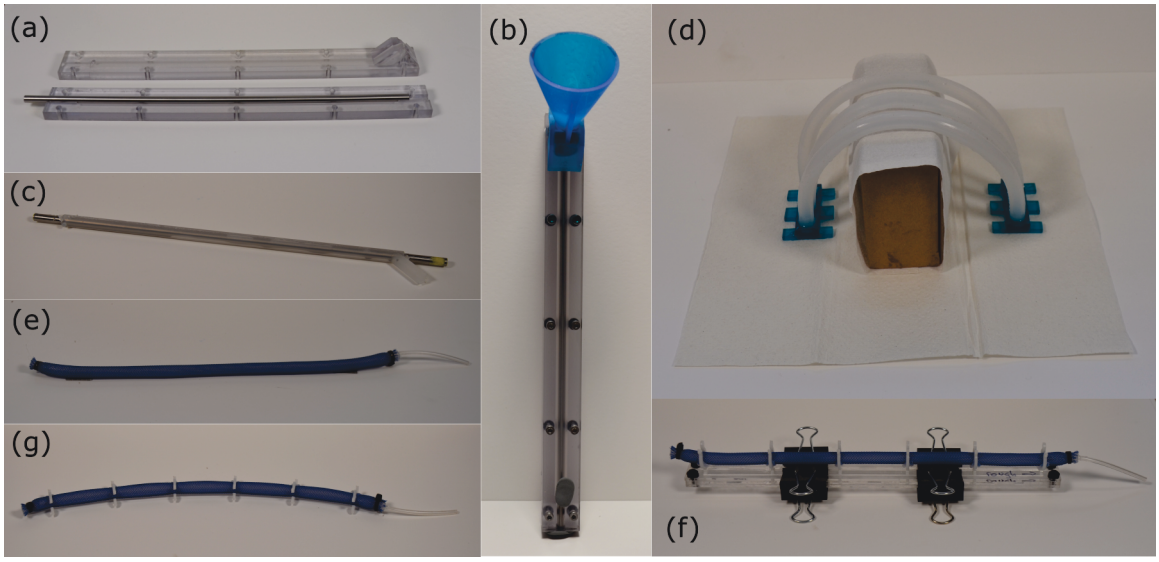

Fig. 2. Visual guide to the manufacturing process steps to complete a McKibben actuator for use in a modular segment, as given in the main text. Shown here are (a) the mold, which was 3D printed on an Object350 Connex2 out of VeroClear, with a stainless steel tight-tolerance mandrel, (b) the funnel assembled to the mold, (c) a cured silicone tube, (d) the capping molds, which were printed out of Tough resin on a Formlabs Form 2, (e) a completed blank McKibben actuator, (f) the key attachment jig, made from laminated laser cut acrylic, and (g) a completed actuator ready for installation into arm.

the bladders were cut to 230 mm, trimming off any small defects at the top and bottom.

7) The bladders were capped with DragonSkin 10, and were allowed to cure without degassing. One mold has a center prominence to set the location of the air inlet tube. See Figure 2.(d).
8) Tubing (1/16" ID) was inserted into one end of the bladder for inflation, and sealed in place with Sil-Poxy. The bladder was then sheathed with the expandable sleeving using a tube jig, shown in Figure 3, and then the sheath was secured with cable ties. See Figure 2.(e).
9) The actuator keys, discussed further in Section III, were secured in a jig used to set the spacing and orientation, and then the actuator was bonded to them using Sil-Poxy (Figure 2.(f)). A completed actuator is shown in Figure 2.(g).

Once established, this process produced relatively small actuators with a low reject rate, though the rate was not specifically measured. Though not required for quality actuators, this method also eliminated almost all leakage from the mold. The funnel is used to contain the silicone during degassing, not to provide extra to account for leakage. The most common causes of rejection were small air bubbles trapped at the bottom of the cavity, or large coalesced air bubbles near the top that didn't fully escape prior to cure. The largest inconsistency came from sheathing, as the process of sheathing stretched the bladders by approximately 25 mm. The key jig limited this variance by setting the distance between each key, and thus each radial support plate.

Fig. 3. The jig used to sheath the bladders with the expandable sleeving. Without the jig, the sheathing constricts around the compliant actuator and sticks before reaching the end. The molded bladder fits inside the tube, while the sheath fits over the outside, and both are pulled away together.

III. SYSTEM DESCRIPTION

The two most important requirements for the arm segment were that it promote pure bending and that it be modular, with the ability to add or remove actuators quickly. To meet these requirements, a radial support plate design was developed, similar to the an existing design [20], but with a greater focus on modularity and providing the correct boundary conditions. In cephalopod arms, transverse muscles support the longitudinal muscles during bending, stiffening to prevent a change in radius, while their physical attachment prevents local rotation [14]. Other existing arms also typically have some method of restraint. Octarm uses circumferential ties [13], and rigid joints have also been used [17].

The radial supports are assembled from three laser cut pieces. The middle layer has cutouts out for the key end, and, when assembled, the keys are trapped between the bottom and top layer, connecting the actuators to the structure and applying a radial and rotational constraint. The radial support assembly is shown in Figure 4. The top plates of the assembly are secured with screws, which means arm variants can be constructed simply by swapping plates or actuators.

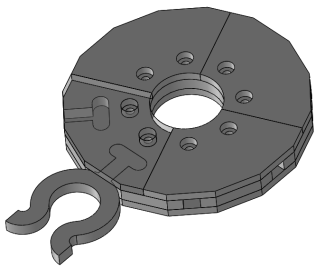

Fig. 4. Solid model of the radial support plate assembly. The bottom and middle plates were laser cut from 1/16" and 3/32" Delrin plastic, and were laminated together with instant adhesive. The top four plates, each of which can secure two actuators, were laser cut from 1/16" transparent acrylic. The holes in the lower assembly were tapped and M3 screws were used to connect the top plates. The keys were also laser cut from 3/32" Delrin.

Six radial support plates were used in each arm segment, and four versions of the plates were produced, with diameters of 45 mm, 60 mm, 75 mm and 90 mm (measured actuator to actuator). Each version, except the 45 mm, had eight actuator cutouts. The 45 mm version had only four due to space constraints. Completed arms are shown in Figure 1 and Figure 5.

Fig. 5. A single-segment arm ready for testing. The lowest radial support plate was bolted to a rigid base, to set a consistent boundary condition. Retroreflective markers were attached to the radial support plate via bracket adapters printed on a FormLabs, replacing the acrylic top plates.

IV. METHODS

Five types of tests were conducted. One test was conducted on individual actuators, and four tests were conducted arm variants. This section describes the methods used, and presents the physical parameters of the variants. A cross reference between variants and tests is given in Section IV-C.

A. Actuator Testing

The keys that connect the actuators to the radial support plates, while essential to the modularity and structure of the arm, partially restrict the radius of the the actuator. To determine the impact of the key design on contraction, three variations of the key design were developed (see Figure 6), differentiated by the amount of actuator circumference bonded to the key.

Three actuators were made with each key design. The original length and contracted length, at an inflation pressure of 103 kPa (15 PSIG), of each actuator was measured with a ruler. The length of any given actuator was observed to change very little above 70 kPa, and testing at 103 kPa provided a stable length. Measurements were taken before and after the keys were attached. The lengths were converted to a percent contraction pre- and post-keys, as well a contraction loss. The results are presented in Section V-A.

B. Arm Testing

Four arm segment tests were developed to study the connection between arm design variables and quantifiable arm performance. Even without knowledge of a specific task, it is reasonable to assume that a given soft arm would need to manipulate an object of a certain size, shape and mass within a workspace. The selected tests seek to identify the bend radius and direction, lateral stiffness and whole-segment contraction, as a simplified means of representing the possible states of a segment, which determines the workspace an arm built from multiple segments can reach. This test set-up most closely matches the set-up used in [21], though this work, in addition to testing a significantly different arm, tests multiple arm variants.

The arm segments were tested within an OptiTrack booth with retroreflective markers attached, as in Figure 5. The system tracks and exports the marker locations, not a capture of the entire arm shape. Two different sizes of markers were used, and most variants had six markers arranged as shown in Figure 5. The 60mm-3 test articles (see Section IV-C) were tested with three markers, due to their compliancy.

The four tests are:

1) *Single Section Free Hang* This test was conducted by holding an unpressurized segment perpendicular to gravity and allowing it to droop to its natural shape. The base was secured, but no additional support was provided. This test provides a simple passive stiffness measurement, which correlates to resistance to load.
2) *Segment Contraction* This test was conducted with the segment upright, and two diametrically opposed actuators (regardless of the total number of actuators) were pressurized to the same value. This test provides a measure of contraction, but also gauges how diametrically opposed actuators change the segment shape.
3) *Single Actuator Bending* This test was conducted with the segment upright, and a single actuator was inflated to a given pressure. Because the test set-up did not include a method synchronizing pressure and position

data, the actuator was held at the desired, measured, pressure for a few seconds, to create an identifiable feature in the data set. This test measures the range of radii and direction possible with single-actuator bends.

4) *Double Actuator Bending* This test pressurized two actuators in sequence. Once the first actuator reached the desired pressure, a second actuator was pressurized. Rather than holding pressures, though, the movement was made continuously. This test provides insight into how radius and direction are interrelated.

All measurements were repeated three times. The position error from the OptiTrack booth is on the order of a fraction of a millimeter, and was neglected. Single actuator bending runs were not accepted unless the position data had a standard deviation of less than 2 mm, to minimize error due to pressure variance. Note that this requirement does not apply to double actuator testing, as that test was conducted dynamically. Data analysis was performed by first transforming the data to an actuator-centric coordinate-system using the two lowest markers. The plane of the bend was identified by grouping the six markers into two vertical sets of three, and fitting a line within the ground plane. A circle was fit to each of the sets within the plane formed by the bend line and the vertical axis. The circle center was constrained to the actuator base, assuming tangency and constant curvature. Constant curvature produced acceptable fits and reduced the shape of the segment to a single, easily compared value.

C. Test Articles

The seven arm variants tested, listed in Table I, cover a range of diameters and the number of actuators per segment. While some soft bending arms have begun to use more than three parallel longitudinal actuators [11], [13], most use only three, in contrast to biological systems. Varying numbers of actuators within a given segment were tested to begin to address this disparity. The layouts selected for each variant, including their marker locations, are shown in Figure 7.

The diameter and number of actuators is encoded in the name of each variant. *60mm-3* means a 60 mm arm diameter measured actuator to actuator, with three actuators around the circumference. Table I also provides a cross reference for which variants were used in which tests. Most notably, the 60mm-6, 45mm-4 and 60mm-3 contraction results were excluded because the arm bent instead of contracting. This result is discussed further in Section V-C.

TABLE I
TEST ARTICLES

Name	Free Hang	Contraction	Single Actuator	Double Actuator
90mm-4	Yes	Yes	Yes[2]	No
75mm-4	Yes	Yes	Yes[2]	No
60mm-8	Yes	Yes	Yes	Yes[3]
60mm-6	Yes	No (bends)	Yes	No
60mm-4	Yes	Yes	Yes[2]	No
60mm-3	Yes[1]	No (bends)	Yes	No
45mm-4	Yes	No (bends)	Yes[2]	No

[1] Tested in both the short and tall orientations.
[2] Tested at 0.5 PSI (3.5 kPa) intervals. If not marked, 2.5 PSI (17.2 kPa) intervals were used.
[3] Only the 60mm-8 was used for this test because it could be used to simulate the effect of more sparse actuators without changing the stiffness.

V. RESULTS

A. Impact of Key Design

The three key designs tested are shown in Figure 6. The smallest, the 1/4 key, restricts the diameter the least, but correspondingly provides the weakest connection. The results of the testing are shown in Table II. The average contracted length prior to key installation was 74.9%, which is acceptable for McKibben actuators. The standard deviation across the actuators was 1.41%, and this variance likely comes from the sheathing installation. The sheaths stretch the inner bladders some amount, but, even with this stretch, the variance in contracted length is small.

TABLE II
ACTUATOR PERCENT LENGTH AFTER CONTRACTION

Type	Article	Before Keys	After Keys	Loss
1/4	1	74.4%	76.9%	-1.54%
1/4	2	75.4%	75.4%	-0.00%
1/4	3	78.0%	77.4%	+0.59%
1/2	1	75.2%	77.1%	-1.96%
1/2	2	74.5%	75.2%	-0.63%
1/2	3	73.2%	74.8%	-1.59%
3/4	1	75.9%	81.3%	-5.46%
3/4	2	73.1%	79.2%	-6.12%
3/4	3	74.2%	78.0%	-3.82%

Though the 1/4 key and 1/2 key showed negligible interference with contraction, while the 3/4 key showed notable interference, the 3/4 key was selected for practical considerations. This design provides the largest bonding surface and entrapped the actuator during bonding. While testing individual actuators, a significant different in bond resilience was noted between the 1/4 key, 1/2 key and 3/4 key. During handling, 1/4 and 1/2 keys frequently disbonded. The 3/4 key was selected to reduce the chance of damaging an arm segment during testing.

B. Single Section Free Hang

The results for the free hang tests are shown in Figure 8. Because the segments were tested with a gravity load, mass and deflection are coupled. Each added actuator or increase in diameter must resist more than it loads, which

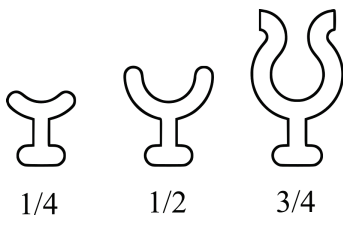

Fig. 6. The three key designs tested. The smallest encompasses approximately a quarter of the actuator circumference, while the largest encompasses approximately three quarters.

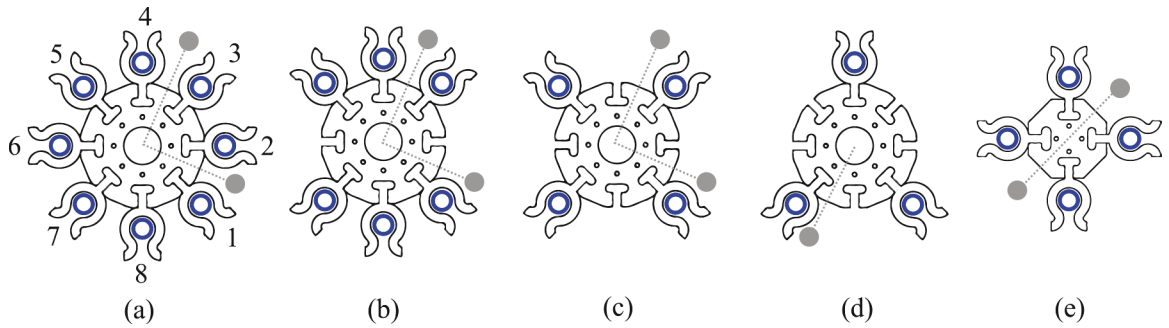

Fig. 7. Actuator layouts for different arm variants, with actuators shown in blue and the planar arrangement of OptiTrack markers shown in silver. (a) This eight-actuator configuration was tested only in a 60 mm diameter, and the numbering shown is referenced in the double actuator test results. (b) This six-actuator layout was tested only as a 60 mm diameter. (c) This four-actuator layout was used for 90mm-4, 75mm-4 and 60mm-4. (d) The three-actuator configuration used only three OptiTrack markers in the entire segment, instead of six. (e) The 45 mm diameter segment was too small to fit eight cutouts, so a modified plate was used with only four. Otherwise, the design remained the same.

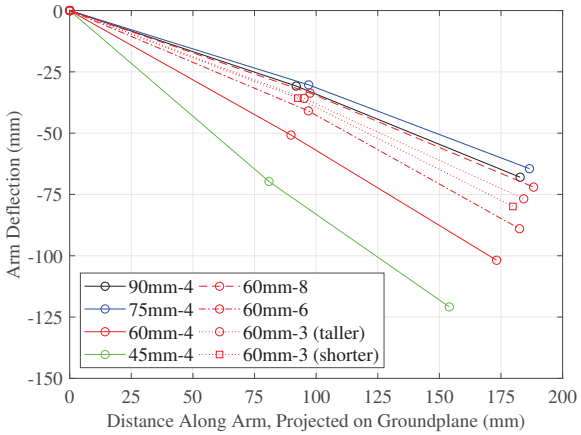

Fig. 8. The deflected state of the tested segments. The positions of each of the upper most set of retroreflective markers are marked and connected by straight lines for visualization. The 60mm-3 section had only three markers instead of six, which reduced segment weight, and cannot be directly compared to the other variants.

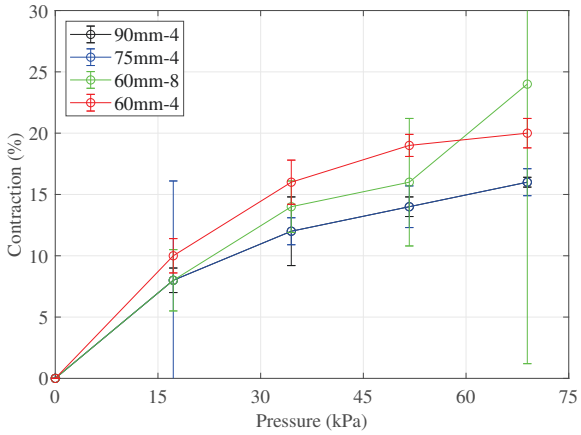

Fig. 9. Contraction of a single segment for four pressures. Markers indicate the data points taken, while the error bars are calculated from the standard deviation between the three trials on each segment. The error is sporadically high due to intermittent marker loss or occlusion in the OptiTrack system.

is likely why the 90mm-4 and 75mm-4 segments performed similarly. With the exception of the 60mm-3 results, adding actuators generally increased stiffness. The 60mm-3 segment had only three retroreflective markers mounted on it, and should not be compared directly to the 60mm-8, -6 or -4, which had six markers. Additionally, the 60mm-3 cross section was not an equilateral triangle, and, thus, had a taller and a shorter orientation. However, the taller and shorter orientation deflected similarly. The 60mm-6 cross section was tested as shown in Figure 7, while the 60mm-4 cross section was tested as a box and not a diamond, exacerbating the difference in cross sectional stiffness.

C. Contraction

The segment contraction results are presented in Figure 9. Initially, all segments with symmetric actuators were planned to be tested, but bending was observed in several of the smaller diameters. No bending was observed during testing of the 90mm-4 and 75mm-4 variants, and the results are effectively indistinguishable.

Significant bending was observed during testing of the 45mm-4 (not plotted), but was attributed to an initial lean exacerbated by contraction. However, closer analysis of the 60mm-6 contraction data (not plotted) and the 60mm-4 data (plotted in Figure 9) showed, respectively, an approximately 2 cm and 1.5 cm drift between the lowest and highest marker when projected onto the ground plane. The drift suggests that those segments did bend, and may be the cause of the higher contraction measured in the 60mm-4 segment. Bending caused by contraction of diametrically opposed actuators suggests that, as the actuators changed length and thus stiffness, the neutral axis of the segment shifted upward, until the mid-line actuators were beneath it.

D. Bend Radius & Direction

The position data gathered for the single and double actuator bend tests was used to calculate a bend radius and direction. The single actuator bend radius results are shown in Figure 10 and Figure 11. The trends observed fit with standard engineering practice: Decreasing the diameter or the number of actuators (decreasing the geometric stiffness)

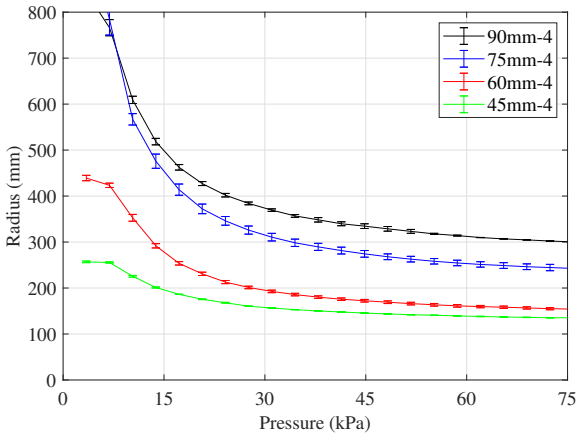

Fig. 10. Bend radius plotted against pressure in a single actuator, for four diameter variants. Measurements were collected every 3.5 kPa (0.5 PSI). The error bars represent the standard deviation of three runs.

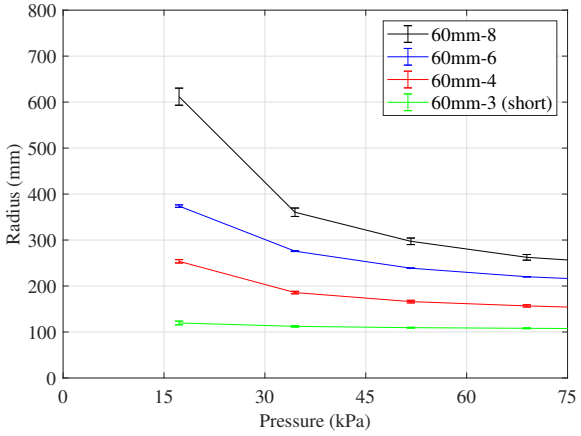

Fig. 11. Bend radius plotted against pressure for four 60mm-diameter-arms, each with a different number of actuators. Measurements were taken every 17.2 kPa (2.5 PSI). The measurements for the 60mm-4 segment are downsampled from Figure 10.

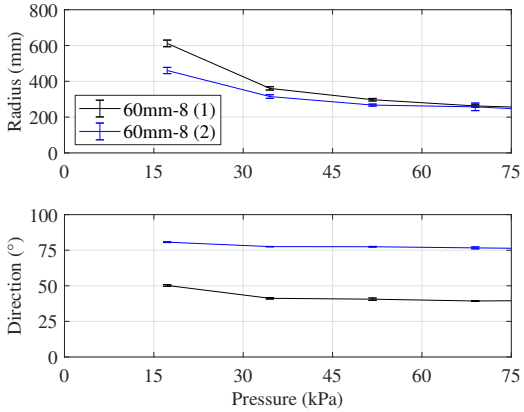

Fig. 12. The bend radius and direction measured from two different single actuator bending tests on the same 60mm-8 segment. Measurements were taken every 17.2 kPa (2.5 PSI).

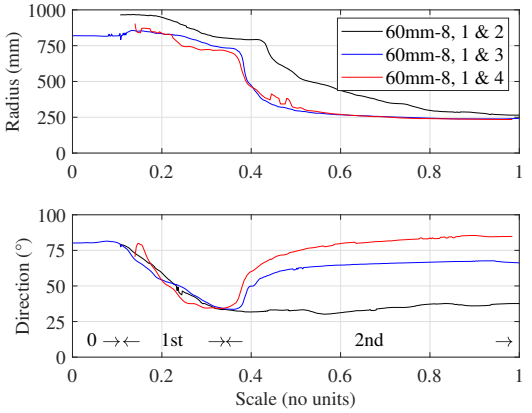

Fig. 13. Double activation bend radius and direction for three actuators pairs on the 60mm-8 segment. The first actuator was pressurized to 17.2 kPa (2.5 PSI), and the second to 68.9 kPa (10 PSI). Because pressure data was not synchronized to position data, the data is plotted against a scale bar. The data was scaled on the x-axes for visualization, but not on the y-axes. Approximate zones of activation are marked on the direction plot.

decreases the minimum bend radius achieved. These graphs also show that the arm segments follow the nonlinear force-profile of McKibben actuators, generating large amounts of bending initially, and then tapering to a static position even as pressure increases.

Bending caused some change in direction in all cases. Two adjacent actuators of the 60mm-8 variant were pressurized separately, to isolate potential actuator variance. The bend radius and diameter are shown in Figure 12. The two cases converge to the same radius but not the same direction, and the magnitude of the direction change is not the same.

Next, two actuators were pressurized in sequence in order to investigate the coupling between bend radius and diameter. The double actuation results are shown in Figure 13. The pairs tested correspond to the actuator numbering shown in Figure 7. Though tested on only one segment, the three pairs mimic the behavior of segments with few actuators.

The initial direction change, nearly identical on all three pairs, was caused by pressurizing the first actuator. Pressurizing the second actuators yielded different results in each of the pairs, even though the end pressure was the same. The larger the angular gap between the pair, so long as it remains less than 180°, the greater the change in direction. The segment radii converge between pairs, as it did with the single actuator testing, but the directions do not.

The authors propose that the amount of direction change is determined by the angular distance between the starting point, which may change due to weight imbalances from markers or sensors, and some stress-resolved position for a given actuator and pressure. In this view, the actuators are not imparting a motion as much as driving the segment to a state where actuator forces after pressurization balance again. Unlike traditional robots, the new state cannot be calculated by adding a known position change to the current state.

VI. APPLICATIONS AND CONCLUSIONS

The first step to designing a functional robot is understanding the relationship between the requirements and accessible design variables. This step is a common barrier in soft robotics, as it requires a detailed understanding of nonlinear materials and large deformation systems. This paper has sought to address one facet of this gap, by examining how the physical parameters of soft bending arms, specifically arm radius and number of actuators, affect stiffness, segment contraction and bend radius and direction. A trade-off was identified between arm stiffness and minimum bend radius, as was coupling between the bend radius and direction. The interrelation of bend radius and direction suggests that soft arms of this type are best thought of as stress-resolved systems, rather than additive systems. Segments with more than three parallel actuators allowed finer directional control when adjacent actuators were pressurized, as the same pressure range was mapped to a smaller actuation space.

This work may be immediately applied to the development of new soft bending arms, with one or multiple segments. The results affirm the advantages of the conical shape of octopus arms, as the larger diameter at the base provides support, while the smaller tip allows dexterity in manipulation. During testing, an arm was built to demonstrate this, and the modularity of the design, and is shown in Figure 14.

The next step in this work is to generalize the relationships, using the experimental results to guide development of a reduced order model that can be used to guide development of more effective soft bending arms.

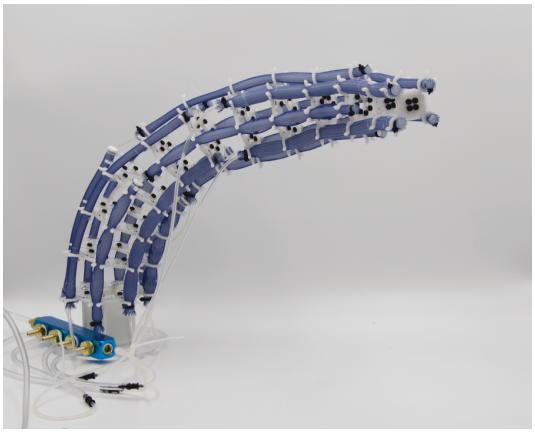

Fig. 14. A demonstration arm built from radial support plates that decrease in diameter toward the tip. The arm has three segments which overlap on two radial support plates.

ACKNOWLEDGMENT

This work was supported by the National Science Foundation, under award IIS-1734627. The authors also thank Dr. Julie Adams for her editorial assistance.

REFERENCES

[1] H. Zhao, K. O'Brien, S. Li, and R. Shepherd, "Optoelectronically innervated soft prosthetic hand via stretchable optical waveguides," *Science Robotics*, vol. 1, 2016.

[2] J. Frame, N. Lopez, O. Curet, and E. Engeberg, "Thrust force characterization of free-swimming soft robotc jellyfish," *Bioinpiration & Biomimetics*, vol. 13, 2018.

[3] T. Umedachi, V. Vikas, and B. Trimmer, "Softworms: the design and control of non-pneumatic, 3d-printed, deformable robots," *Bioinpiration & Biomimetics*, vol. 11, 2016.

[4] M. Wooten and I. Walker, "A novel vine-like robot for in-orbit inspection," *45th International Conference on Environmental Systems (ICES 2015)*, 2015.

[5] M. Cianchetti, T. Ranzani, G. Gerboni, I. D. Falco, C. Laschi, and A. Menciassi, "Stiff-flop surgical manipulator: mechanical design and experimental characterization of the single module," *IEEE/RSJ International Conference on Intelligent Robots and Systems (IROS 2013)*, 2013.

[6] L. A. Abeach, S. Nefti-Meziani, and S. Davis, "Design of a variable stiffness soft dexterous gripper," *Soft Robotics*, vol. 4, no. 3, pp. 274–284, 2017.

[7] R. Shepherd, F. Ilievski, W. Choi, S. Morin, A. Stokes, A. Mazzeo, X. Chen, M. Wang, and G. Whitesides, "Multigait soft robot," *Proceedings of the National Academy of Sciences of the United States of America (PNAS)*, vol. 108, no. 51, 2011.

[8] O. Yirmibesoglu, J. Morrow, S. Walker, W. Gosrich, R. Canizares, H. Kim, U. Daalkhaijav, C. Fleming, C. Branyan, and Y. Menguc, "Direct 3d printing of silicone elastomer soft robots and their performance comparison with molded counterparts," *IEEE International Conference on Soft Robotics (RoboSoft 2018)*, 2018.

[9] C. Branyan, C. Fleming, J. Remaley, A. Kothari, K. Tumer, R. Hatton, and Y. Menguc, "Soft snake robots: Mechanical design and geometric gait implementation," *IEEE Conference on Robotics and Biomimetics (RoBio 2017)*, 2017.

[10] J. Fras, M. Macias, Y. Noh, and K. Althoefer, "Fluidical bending actuator designed for soft octopus robot tentacle," *IEEE International Conference on Soft Robotics (RoboSoft 2018)*, 2018.

[11] M. Giannaccini, C. Xiang, A. Atyabi, T. Theodoridis, S. Nefti-Meziani, and S. Davis, "Novel design of a soft lightweight pneumatic continuum robot arm with decoupled variable stiffness and positioning," *Soft Robotics*, vol. 5, no. 1, 2018.

[12] W. Zhang and P. Polygerinos, "Distributed planning of multi-segment soft robotic arms," *Annual American Control Conference (ACC 2018)*, 2018.

[13] I. Walker, D. Dawson, T. Flash, F. Grasso, R. Hanlon, B. Hochner, W. Kier, C. Pagano, C. Rahn, and Q. Zhang, "Continuum robot arms inspired by cephalopods," *Proceedings SPIE Conference on Unmanned Ground Vehicle Technology VII*, pp. 303–314, 2005.

[14] W. Kier and K. Smith, "Tongues, tentacles and trunks: the biomechanics of movement in muscular-hydrostats," *Zoological Journal of the Linnean Society*, vol. 83, no. 4, pp. 307–324, 1985.

[15] A. Mishra, A. Mondini, E. D. Dottore, A. S. 1, F. Tramacere, and B. Mazzolai, "Modular continuum manipulator: Analysis and characterization of its basic module," *Biomimetics*, vol. 3, 2018.

[16] T. Doi, S. Wakimoto, K. Suzumori, and K. Mori, "Proposal of flexible robotic arm with thin mckibben actuators mimicking octopus arm structure," *IEEE/RSJ International Conference on Intelligent Robots and Systems (IROS 2016)*, pp. 5503–5508, 2016.

[17] E. Guglielmino, N. Tsagarakis, and D. Caldwell, "An octopus anatomy-inspired robotic arm," *IEEE/RSJ International Conference on Intelligent Robots and Systems (IROS 2010)*, 2010.

[18] M. Follador, M. Cianchetti, and C. Laschi, "Development of the functional unit of a completely soft octopus-like robotic arm," *4th IEEE RAS & EMBS International Conference on Biomedical Robotics and Biomechatronics (BioRob 2012)*, 2012.

[19] M. Cianchetti, M. Follador, B. Mazzolai, P. Dario, and C. Laschi, "Design and development of a soft robotic octopus arm exploiting embodied intelligence," *IEEE International Conference on Robotics and Automation (ICRA 2012)*, 2012.

[20] Y. Ansari, M. Manti, E. Falotico, M. Cianchetti, and C. Laschi, "Multiobjective optimization for stiffness and position control in a soft robot arm module," *IEEE Robotics and Automation Letters*, vol. 3, 2018.

[21] Y. S. adn S. Song, X. Liang, and H. Ren, "A miniature soft robotic manipulator based on novel fabrication methods," *IEEE Robotics and Automation Letters*, vol. 1, 2016.